International Journal of analytical and Numerical Methods in Mechanical Design
Winter & Spring 2023 Vol 2 , Issue 1, 37-47

Nonlinear buckling analysis of clamped-free porous FG sandwich beams with temperature dependent materials

Mohsen Rahmani [a], ✉

[a] Department of Mechanics, Tuyserkan Branch, Islamic Azad University, Tuyserkan, Iran
Received 10 March 2023; Revised 10 April 2023; Accepted 10 May 2023
✉ mohsen_rahmani@ymail.com

Abstract

Analysing the buckling behaviour of the two kinds of sandwich beams, the first one with functionally graded material faces and homogeneous core and the second one with functionally graded material core and homogeneous faces are presented in this paper based on a high order sandwich beam theory. Properties of the constituent materials are assumed temperature dependent and functionally graded materials are modelled by a power law rule. Even and uneven porosity distributions are considered to improve the accuracy of the model. Minimum potential energy principle is used to obtain the govern equations and Galerkin method is applied used to solve the equations in a clamped free boundary conditions. Lateral displacement, and thermal stresses of the core and Lagrange strains are considered. To verify the procedure, the results of the present study are compared with the literature. Thickness, length, porosity, wave number and temperature effect on the critical load are investigated too.

Keywords: Functionally graded material; Boundary condition; Porosity; Smart material

1. Introduction

To have a structure with an excellent efficiency, great bending rigidity and light weight, the concept of sandwich which are composed of two firm and slim skins that cover a soft and thick core have been proposed and used in the advanced industries such as reactors, aerospace, construction and satellite. In high temperature environments, using ordinary composite materials and laminates in the sandwich panels leads to delamination, stress concentration and failure. So, to eliminate these problems, the microscopic inhomogeneous functionally graded materials have been used which the properties vary through the thickness smoothly. Since during the manufacturing the FGMs, some micro voids, porosities, are appeared that affect the materials properties, some porosity distributions have been proposed to modify the models of FGM in the analysis. Also, in high thermal conditions, these properties reduces. So, material properties changing with temperature should be considered (Rahmani et al., (2019)-a; Rahmani et al., (2020)-b).

In the classical theories, the core is considered as an inflexible layer, but it is a transversely flexible one, therefore, to accurate investigation of the mechanical behavior of sandwich structures, considering this effect, the sandwich panel high order theory was proposed (Frostig et al., (1992)). Also, by applying various theories, researchers have been interested in analyzing the beams buckling and post-buckling. Mayandi and Jeyaraj studied the mechanical behaviors of FG-CNTR polymer composite beam such as buckling by using finite element method (Mayandi and Jeyaraj, (2015)). Mammano and Dragoni presented the approximate equations of buckled beam based on the elastica solution for low-stiffness elastic suspensions (Scirè Mammano and Dragoni, (2017)). Chai et al. analyzed the buckling and bending responses of laminated composite beam-column based on Euler—Bernoulli beam and classical lamination theory (Chai et al., (2010)). Alijani and et al. studied the elasto-plastic nonlinear buckling responses of FGM beams based on finite element method (Alijani et al., (2015)). Majumdar and Das analyzed the thermal buckling behavior of clamped FG beams based on the Euler-Bernoulli theory (Majumdar and Das, (2018)). Yap et al. investigated the flexural modulus of the laminated composite beam effect on the buckling behavior, based on Euler-Bernoulli beam theory (CW et al., (2008)). Koissin et al. studied the physical nonlinearity effect on the buckling responses of the sandwich beam with a foam core experimentally, theoretically and numerically (Koissin et al., (2010)). Tran et al. studied the bending and buckling behavior of sandwich FG beam based on third order shear deformation theory and finite element method in thermal conditions (Tran et al., (2019)). Osofero et al. investigated the vibration and buckling of FG sandwich beams by using a quasi-3D theories (Osofero et al., (2016)). Challamel and Girhammar studied the buckling behavior of partial composite beam-columns by using the variational theories and by considering the shear and axial effects (Challamel and Girhammar, (2011)). Bhangale and Ganesan analyzed the thermoelastic buckling and vibration behavior of FG sandwich beam with viscoelastic core by using a finite element procedure (Bhangale and Ganesan, (2006)). By applying a unified higher order shear deformation beam theory, Hamed et al. studied the buckling behavior of composite laminated sandwich beam rested on elastic foundation by considering the effect of in-plane varying compressive force (Hamed et al., (2020)). Li et al.

analyzed the thermal post buckling of the negative Poisson's ratio FG sandwich beams with a honeycomb core by using finite element simulations (Li et al., (2019)). Liu et al. studied the thermal-mechanical coupling buckling analysis of porous FG sandwich beams by using the high-order sinusoidal shear deformation theory (Liu et al., (2019)). Paul and Das investigated the nonlinear buckling behavior of tapered FG beam by using Timoshenko beam theory (Paul and Das, (2017)). Malikan studied the buckling of a SWCNT based on the refined beam theory (Malikan, 2019). Almitani studied the buckling behavior of different types of FG beams based on the Euler-Bernoulli beam theory and a finite element model (Almitani, 2018). Fouda et al. investigated the bending, buckling and vibration of FG porous beam based on a finite element model (Fouda et al., 2017). Gao et al. analyzed the buckling behaviors of the FG cylindrical beams with radially and axially varying material in-homogeneities by a high-order cylindrical beam model (Gao et al., 2021). Basaglia and Camotim studied buckling behavior of thin-walled steel structural systems by using the application of beam finite element models based on generalized beam theory for different support conditions and subjected to various loadings (Basaglia and Camotim, 2015). Akbas studied the post-buckling analysis of an edge cracked cantilever beam composed of functionally graded material (FGM) subjected to axial compressive loads by using the total Lagrangian Timoshenko beam element approximation (Akbaş, 2015). Dinzart et al. studied the thermo-mechanical response of beams made up of thermoplastic under cyclic bending. The stability of steady-state solution was done by a perturbation method (Dinzart et al., 2008). Janevski et al. studied the thermal buckling and vibration behavior of Euler-Bernoulli FG nanobeams based on a higher order nonlocal strain gradient theory (Janevski et al., 2020). Magnucki et al. studied the deflection of a laminate sandwich beam under bending (Magnucki et al., 2013).

By reviewing various references, the author decided to investigate the buckling of two kinds of sandwich beams in the uniform temperature distributions for clamped-free boundary conditions, by applying a modified high order sandwich beam theory. There are two FG skins and a homogeneous core in the first model, and two homogeneous skins and a FG core in the second one. FGMs are modelled by a power law rule by considering the porosity distributions. Temperature dependency of all materials is considered. High order and in-plane stresses and lateral flexibility of the core, and thermal stresses of the layers are considered. The minimum potential energy principle and a Galerkin procedure are applied to obtain and solve the equations. To verify the procedure, the results of the present study are compared with the literatures. Thickness, length, porosity, wave number and temperature effect on the critical load are studied.

2. Basic equations

Consider two models of sandwich beams as shown in Fig. 1. There are two FG skins and metal core in the first model, and a FG core with ceramic and metal skins in the second one.

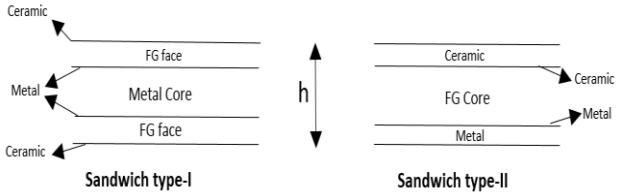

Fig .1. Different sandwich beams with FG layers

It is considered that metal, ceramic and FGMs properties change by temperature based on the following equation (Rahmani et al., (2020)-a):

$$P = P_0\left(P_{-1}T^{-1} + 1 + P_1T + P_2T^2 + P_3T^3\right) \quad (1)$$

Where "P"s are unique thermal coefficients for material properties and "$\Delta T=T-T_0$", which "T_0" is the room temperature. The material properties of FGM by considering even and uneven porosity volume fraction are modelled based on a power law rule. For the sandwich type-I with even porosity the equations are as follows (Rahmani et al., (2020)-a):

$$P_j\left(z_j,T\right) = g\left(z_j\right)P_{ce}^j\left(T\right) + \left[1-g\left(z_j\right)\right]P_m^j\left(T\right) - \left(P_{ce}^j\left(T\right)+P_m^j\left(T\right)\right)\frac{\zeta}{2} \quad (2)$$

$$g\left(z_t\right) = \left(\frac{\frac{h_t}{2}-z_t}{h_t}\right)^N;\ g\left(z_b\right) = \left(\frac{\frac{h_b}{2}+z_b}{h_b}\right)^N;\ j=(t,b) \quad (3)$$

And for type-II is as follows (Rahmani et al., (2020)-a):

$$P_c\left(z_c,T\right) = g\left(z_c\right)P_{ce}^c\left(T\right) + \left[1-g\left(z_c\right)\right]P_m^c\left(T\right) - \left(P_{ce}^c\left(T\right)+P_m^c\left(T\right)\right)\frac{\zeta}{2} \quad (4)$$

$$g\left(z_c\right) = \left(\frac{\frac{h_c}{2}-z_c}{h_c}\right)^N \quad (5)$$

g(z) is ceramic volume fraction; "N" is the nonnegative power law index; "ζ" is the even porosity volume fraction; "c" refers to the core and "t", "b" are top and bottom skins, respectively.

On the other hand, in the modelling of uneven porosity it is considered that the voids are condensed at the middle of the FG layers and there are not voids near the edge of the layers. As a result, for the sandwich type-I, the material properties are modified as follows (Rahmani et al., (2020)-a):

$$P_j\left(z_j,T\right) = g\left(z_j\right)P_{ce}^j\left(T\right) + \left[1-g\left(z_j\right)\right]P_m^j\left(T\right) - \left(P_{ce}^j\left(T\right)+P_m^j\left(T\right)\right)\frac{\zeta}{2}\left(1-\frac{2|z|}{h}\right),\ j=(t,b) \quad (6)$$

And for sandwich type-II, the equation is as follows (Rahmani et al., (2020)-a):

$$P_c\left(z_c,T\right) = g\left(z_c\right)P_{ce}^c\left(T\right) + \left[1-g\left(z_c\right)\right]P_m^c\left(T\right) - \left(P_{ce}^c\left(T\right)+P_m^c\left(T\right)\right)\frac{\zeta}{2}\left(1-\frac{2|z_c|}{h}\right) \quad (7)$$

The equations of buckling behavior of sandwich

beams ore obtained by applying the principle of minimum potential energy (Rahmani et al., (2019)-b):

$$\prod\left(\delta U+\delta V\right)=0 \tag{8}$$

"δV", is the external load potential variation; and "δU" is the total strain energy variation. "δU" is presented as follows which in-plane stresses of the core are considered too.

In "δU", the linear part of strains are considered with mechanical stresses and nonlinear part of strains are considered with thermal stresses. Lagrange multipliers are appeared due to the compatibility constrained which fixed the skins and the core to each other. "d_{xx}" and "d_{zz}" are the nonlinear parts of normal and shear; "σ^{T}_{xx}" and "σ^{T}_{zz}" are the thermal stresses; and "λ_x" and "λ_z" are the Lagrange multipliers. FGMs properties are displacement and temperature.

The variation of the external loads as follows:

$$\delta V=-\int_0^L(P_t\delta w_0^t+P_b\delta w_0^b+n_x^t\delta u_0^t+n_x^b\delta u_0^b)dx \tag{9}$$

$$\begin{aligned}\delta U_p=&\int_{A_t}(\sigma_{xx}^t\delta\varepsilon_{xx}^t+\sigma_{xx}^{tT}\delta d_{xx}^t+\tau_{xz}^t\delta\gamma_{xz}^t\\&+\sigma_{zz}^{tT}\delta d_{zz}^t)dA+\\&\int_{A_b}(\sigma_{xx}^b\delta\varepsilon_{xx}^b+\sigma_{xx}^{bT}\delta d_{xx}^b+\tau_{xz}^b\delta\gamma_{xz}^b\\&+\sigma_{zz}^{bT}\delta d_{zz}^b)dv+\\&\int_{A_{core}}(\sigma_{xx}^c\delta\varepsilon_{xx}^c+\sigma_{xx}^{cT}\delta d_{xx}^c+\sigma_{zz}^c\delta\varepsilon_{zz}^c\\&+\sigma_{zz}^{cT}\delta d_{zz}^c+\tau_{xz}^c\delta\gamma_{xz}^c)dv+\\&\delta\int_0^L[\lambda_{xt}\left(\mathrm{u_t}\left(z_t=\frac{h_t}{2}\right)-u_c\left(z_c=-\frac{h_c}{2}\right)\right)\\&+\lambda_{zt}\left(\mathrm{w_t}-\mathrm{w_c}\left(z_c=-\frac{h_c}{2}\right)\right)+\\&\lambda_{xb}(\mathrm{u_c}\left(z_c=\frac{h_c}{2}\right)-u_b\left(z_b=-\frac{h_b}{2}\right)\\&+\lambda_{zb}\left(\mathrm{w_c}\left(z_c=\frac{h_c}{2}\right)-w_b\right)]dx\end{aligned} \tag{10}$$

"n_x^j" (j=t, b) are the in-plane external loads of the skins; and "P_j" are the lateral distributed loads applied on skins, respectively. The displacement fields of the skins are modelled by the first order shear deformation theory.

$$u_j\left(x,z,t\right)=u_{0j}\left(x,t\right)+z_j\phi_{xj}\ \ j=(t,b) \tag{11}$$

$$w_j\left(x,z,t\right)=w_{0j}\left(x,t\right) \tag{12}$$

where "u_0^j" are the longitudinal and w_0^j(j = t, b) are the lateral displacements of the mid-plane of the skins; "ϕ" is rotation of the normal line of the middle of the layer. The displacement equations of the core are polynomials which contain seven unknown coefficients (Rahmani and Dehghanpour, (2020)):

$$u_c\left(x,z_c,t\right)=u_0\left(x,t\right)+u_1\left(x,t\right)z_c+u_2\left(x,t\right)z_c^2+u_3\left(x,t\right)z_c^3 \tag{13}$$

$$w_c\left(x,z_c,t\right)=w_0\left(x,t\right)+w_1\left(x,t\right)z_c+w_2\left(x,t\right)z_c^2 \tag{14}$$

The strains of the skins are considered based on the Lagrange strain tensor as follows (Rahmani and Dehghanpour, (2020)):

$$\varepsilon_{xx}^j=u_{j,x}+\frac{1}{2}\left(w_{0j,x}\right)^2-\alpha_j\Delta T_j,\ j=(t,b) \tag{15}$$

$$\varepsilon_{zz}^j=\frac{1}{2}\phi_{jx}^2-\alpha_j\Delta T_j \tag{16}$$

$$\begin{aligned}\gamma_{xz}^j\left(x,z_j,t\right)=&u_{j,z}(x,t)+w_{j,x}(x,t)+\\&u_{j,x}(x,t)u_{j,z}(x,t)+w_{j,x}(x,t)w_{j,z}(x,t)\end{aligned} \tag{17}$$

The strains components in the core are presented as:

$$\varepsilon_{xx}^c\left(x,z_c,t\right)=u_{c,x}\left(x,z_c,t\right)+\frac{1}{2}\left(w_{0c,x}\right)^2-\alpha_c\Delta T \tag{18}$$

$$\varepsilon_{zz}^c\left(x,z_c,t\right)=w_{c,z}\left(x,z_c,t\right)+\frac{1}{2}\left(\phi_{0c}\right)^2+\frac{1}{2}\left(w_{1c}\right)^2-\alpha_c\Delta T \tag{19}$$

$$\gamma_{xz}^c\left(x,z_c,t\right)=u_{c,z}(x,z_c,t)+w_{c,x}(x,z_c,t)+w_{1c}w_{0c,x} \tag{20}$$

In Eq. (9) and Eq. (10), all parameters are replaced with displacement of the core and skins and by using the compatibility conditions and some algebraic operations, thirteen equations are derived:

$$u_{0t}+\frac{h_t}{2}\phi^t=u_{0c}-\frac{h_c}{2}\phi_0^c+\frac{h_c^2}{4}u_{2c}-\frac{h_c^3}{8}u_{3c} \tag{21}$$

$$w_{0t}=+w_{0c}-\frac{h_c}{2}w_{1c}+\frac{h_c^2}{4}w_{2c} \tag{22}$$

$$u_{0b}-\frac{h_b}{2}\phi^b=u_{0c}+\frac{h_c}{2}\phi_0^c+\frac{h_c^2}{4}u_{2c}+\frac{h_c^3}{8}u_{3c} \tag{23}$$

$$w_{0b}=+w_{0c}+\frac{h_c}{2}w_{1c}+\frac{h_c^2}{4}w_{2c} \tag{24}$$

Based on the Eqs. (21-24) the skins displacements are dependent to the core ones, so the unknown decrease to nine and the number of the governing equations are nine.

$$+\frac{h_t}{2}N_{x,x}^t-M_{x,x}^t+N_z^{tT}\phi_x^t+N_{xz}^t+\frac{h_t}{2}n_x^t=0 \tag{25}$$

$$-\frac{h_b}{2}N_{x,x}^b-M_{x,x}^b+N_z^{bT}\phi_x^b+N_{xz}^b-\frac{h_b}{2}n_x^b=0 \tag{26}$$

$$-N_{x,x}^t-N_{x,x}^b-N_{x,x}^c-n_x^t-n_x^b=0 \tag{27}$$

$$\begin{aligned}&+\frac{h_c}{2}N_{x,x}^t-\frac{h_c}{2}N_{x,x}^b-M_{1,x}^c+N_z^{cT}\phi_0^c+N_{xz}^c+\\&\frac{h_c}{2}n_x^t-\frac{h_c}{2}n_x^b=0\end{aligned} \tag{28}$$

$$-\frac{h_c^2}{4}N^{t}_{x,x}-\frac{h_c^2}{4}N^{b}_{x,x}-M^{c}_{2,x}+2M^{c}_{xz\,1}-\frac{h_c^2}{4}n^{t}_{x}-\frac{h_c^2}{4}n^{b}_{x}=0 \quad (29)$$

$$+\frac{h_c^3}{8}N^{t}_{x,x}-\frac{h_c^3}{8}N^{b}_{x,x}-M^{c}_{3,x}+3M^{c}_{xz\,2}+\frac{h_c^3}{8}n^{t}_{x}-\frac{h_c^3}{8}n^{b}_{x}=0 \quad (30)$$

$$-N^{t}_{x}(w^{c}_{0})+\frac{h_c}{2}N^{t}_{x}(w^{c}_{1})-\frac{h_c^2}{4}N^{t}_{x}(w^{c}_{2})-N^{tT}_{x,x}w^{c}_{0,x}-N^{tT}_{x}w^{c}_{0,xx}+\frac{h_c}{2}N^{tT}_{x,x}w^{c}_{1,x}+\frac{h_c}{2}N^{tT}_{x,x}w^{c}_{1,x}-\frac{h_c^2}{4}N^{tT}_{x,x}w^{c}_{2,x}-\frac{h_c^2}{4}N^{tT}_{x}w^{c}_{2,xx}-N^{t}_{xz,x}-N^{b}_{x}(w^{c}_{0})-\frac{h_c}{2}N^{b}_{x}(w^{c}_{1})-\frac{h_c^2}{4}N^{b}_{x}(w^{c}_{2})-N^{bT}_{x,x}w^{c}_{0,x}-N^{bT}_{x}w^{c}_{0,xx}-\frac{h_c}{2}N^{bT}_{x,x}w^{c}_{1,x}-\frac{h_c}{2}N^{bT}_{x,x}w^{c}_{1,x}-\frac{h_c^2}{4}N^{bT}_{x,x}w^{c}_{2,x}-\frac{h_c^2}{4}N^{bT}_{x}w^{c}_{2,xx}-N^{b}_{xz,x}-N^{c}_{xz,x}-N^{c}_{x}(w^{c}_{0})-N^{cT}_{x,x}w^{c}_{0,x}-N^{cT}_{x}w^{c}_{0,xx}-P_t-P_b=0 \quad (31)$$

$$+\frac{h_c}{2}N^{t}_{x}(w^{c}_{0})-\frac{h_c^2}{4}N^{t}_{x}(w^{c}_{1})+\frac{h_c^3}{8}N^{t}_{x}(w^{c}_{2})+\frac{h_c}{2}N^{tT}_{x,x}w^{c}_{0,x}+\frac{h_c}{2}N^{tT}_{x}w^{c}_{0,xx}-\frac{h_c^2}{4}N^{tT}_{x,x}w^{c}_{1,x}-\frac{h_c^2}{4}N^{tT}_{x,x}w^{c}_{1,xx}+\frac{h_c^3}{8}N^{tT}_{x,x}w^{c}_{2,x}+\frac{h_c^3}{8}N^{tT}_{x}w^{c}_{2,xx}+\frac{h_c}{2}N^{t}_{xz,x}-\frac{h_c}{2}N^{b}_{x}(w^{c}_{0})-\frac{h_c^2}{4}N^{b}_{x}(w^{c}_{1})-\frac{h_c^3}{8}N^{b}_{x}(w^{c}_{2})-\frac{h_c}{2}N^{bT}_{x,x}w^{c}_{0,x}-\frac{h_c}{2}N^{bT}_{x}w^{c}_{0,xx}-\frac{h_c^2}{4}N^{bT}_{x,x}w^{c}_{1,x}-\frac{h_c^2}{4}N^{bT}_{x,x}w^{c}_{1,xx}-\frac{h_c^3}{8}N^{bT}_{x,x}w^{c}_{2,x}-\frac{h_c^3}{8}N^{bT}_{x}w^{c}_{2,xx}-\frac{h_c}{2}N^{b}_{xz,x}+N^{c}_{z}+N^{c}_{z}+N^{cT}_{z}w^{c}_{1}-M^{c}_{xz\,1,x}+\frac{h_c}{2}P_t-\frac{h_c}{2}P_b=0 \quad (32)$$

$$-\frac{h_c^2}{4}N^{t}_{x}(w^{c}_{0})+\frac{h_c^3}{8}N^{t}_{x}(w^{c}_{1})-\frac{h_c^4}{16}N^{t}_{x}(w^{c}_{2})-\frac{h_c^2}{4}N^{tT}_{x,x}w^{c}_{0,x}-\frac{h_c^2}{4}N^{tT}_{x}w^{c}_{0,xx}+\frac{h_c^3}{8}N^{tT}_{x,x}w^{c}_{1,x}+\frac{h_c^3}{8}N^{tT}_{x,x}w^{c}_{1,x}-\frac{h_c^4}{16}N^{tT}_{x,x}w^{c}_{2,x}-\frac{h_c^4}{16}N^{tT}_{x}w^{c}_{2,xx}-\frac{h_c^2}{4}N^{t}_{xz,x}-\frac{h_c^2}{4}N^{b}_{x}(w^{c}_{0})-\frac{h_c^3}{8}N^{b}_{x}(w^{c}_{1})-\frac{h_c^4}{16}N^{b}_{x}(w^{c}_{2})-\frac{h_c^2}{4}N^{bT}_{x,x}w^{c}_{0,x}-\frac{h_c^2}{4}N^{bT}_{x}w^{c}_{0,xx}-\frac{h_c^3}{8}N^{bT}_{x,x}w^{c}_{1,x}-\frac{h_c^3}{8}N^{bT}_{x,x}w^{c}_{1,x}-\frac{h_c^4}{16}N^{bT}_{x,x}w^{c}_{2,x}-\frac{h_c^4}{16}N^{bT}_{x}w^{c}_{2,xx}-\frac{h_c^2}{4}N^{b}_{xz,x}+2M^{c}_{z}-M^{c}_{xz\,2,x}-\frac{h_c^2}{4}P_t-\frac{h_c^2}{4}P_b=0 \quad (33)$$

In the skins equations, "N"s, "M"s and "N_{xz}"s refer the in-plane stress resultants, the moment resultants and the out of plane shear stress resultants, respectively, which presented as follows (Rahmani and Dehghanpour, (2020)):

$$N^{j}_{xx}=A_{11}u^{j}_{0,x}+B_{11}\phi^{j}_{,x}-N^{jT}_{xx},\ j=(t,b) \quad (34)$$

$$M^{j}_{xx}=B_{11}u^{j}_{0,x}+D_{11}\phi^{j}_{,x}-M^{jT}_{xx} \quad (35)$$

$$N^{j}_{xz}=\pi^2/12\,A_{44}(\phi^{j}+w^{j}_{0,x}) \quad (36)$$

"A", "B" and "D" are the constant coefficients of stretching, the bending-stretching, and bending stiffness:

$$\begin{Bmatrix}A^{j}_{11}\\B^{j}_{11}\\D^{j}_{11}\end{Bmatrix}=\int_{-hj/2}^{hj/2}\left(\frac{E_j}{1-\nu_j^{\,2}}\right)\begin{Bmatrix}1\\z_j\\z_j^{\,2}\end{Bmatrix}dz_j \quad (37)$$

$$\{A^{j}_{44}\}=\int_{-hj/2}^{hj/2}\left(\frac{E_j}{1+2\nu_j}\right)dz_j$$

"N^{T}" and "M^{T}" display the thermal high order stress and momentum resultants in the skins:

$$\begin{Bmatrix}N^{jT}_{xx},N^{jT}_{zz}\\M^{jT}_{xx}\end{Bmatrix}=-\int_{-hj/2}^{hj/2}\left(\frac{E_j}{1-\nu_j}\alpha_j T_j\right)\begin{Bmatrix}1\\z_j\end{Bmatrix}dz_j,\quad j=(t,b,c) \quad (38)$$

"E", "ν" and "α" are the Elastic modulus, the Poisson's ratio and the thermal expansion coefficient, respectively. The high order stress resultants in the core can be defined as follows:

$$N_{xzc},M_{xz\,1},M_{xz\,2}=\int_{-hc/2}^{hc/2}\left(1,z_c,z_c^{\,2}\right)\tau^{c}_{xz}dz_c \quad (39)$$

$$N_{zc},M_{zc}=\int_{-hc/2}^{hc/2}\left(1,z_c\right)\sigma^{c}_{zz}dz_c \quad (40)$$

$$N^{c}_{x},M^{c}_{1},M^{c}_{2},M^{c}_{3}=\int_{-hc/2}^{hc/2}\left(1,z_c,z_c^{\,2},z_c^{\,3}\right)\sigma^{c}_{xx}dz_c \quad (41)$$

On the other hand, $N_x^j(w_l^c)$ is (Kheirikhah et al., (2012)):

$$N_x^j(w_l^c) = N_{x,x}^j w_{l,x}^c + N_x^j w_{l,xx}^c ; \quad j=(t,b,c), l=(0,1,2) \tag{42}$$

where $\widehat{N}_x^j$ are the in-plane external loads applied to the skins and the core, which are the parts of total external load, $\widehat{N}_0$, as follows:

$$N_x^t + N_x^b + N_x^c = -N_0 \tag{43}$$

The uniform state of strain for the face sheets and the core is considered. At edges 'x=0" or "x=L" and with a little simplification the equilibrium equations are presented as:

$$\frac{N_x^t}{h_t\bar{E}_t} = \frac{N_x^b}{h_b\bar{E}_b} = \frac{N_x^c}{h_c\bar{E}_c} \tag{44}$$

where $\bar{E}_j$ is the equilibrium elasticity modulus of the layers that are defined as:

$$\bar{E}_j = \frac{\int_{-h_j/2}^{h_j/2} E_j(z_j)dz_j}{h_j}; \quad j=(t,b,c) \tag{45}$$

Hence, by using of Eq. (44) and (45), the in-plane external loads applied to the face sheets and the core along the "x" direction can be obtained as:

$$\begin{Bmatrix} N_x^t \\ N_x^b \\ N_x^c \end{Bmatrix} = \frac{-N_0}{h_t\bar{E}_t + h_b\bar{E}_b + h_c\bar{E}_c} \begin{Bmatrix} h_t\bar{E}_t \\ h_b\bar{E}_b \\ h_c\bar{E}_c \end{Bmatrix} \tag{46}$$

3. Galerkin method and the numerical results

To solve the buckling equations of sandwich beams, Galerkin method is used for clamped free boundary condition. Nine shape functions of this state is presented as(Rahmani and Mohammadi, (2021)):

$$\phi_x^j = C_{\phi xj}\frac{\lambda_m}{L}\left(\sinh\left(\frac{\lambda_m x}{L}\right)+\sin\left(\frac{\lambda_m x}{L}\right)-\gamma_m\left(\cosh\left(\frac{\lambda_m x}{L}\right)-\cos\left(\frac{\lambda_m x}{L}\right)\right)\right)e^{i\omega t}, \quad j=(t,b) \tag{47}$$

$$u_{ck} = C_{uk}\frac{\lambda_m}{L}\left(\sinh\left(\frac{\lambda_m x}{L}\right)+\sin\left(\frac{\lambda_m x}{L}\right)-\gamma_m\left(\cosh\left(\frac{\lambda_m x}{L}\right)-\cos\left(\frac{\lambda_m x}{L}\right)\right)\right)e^{i\omega t}, \quad k=(0,1,2,3) \tag{48}$$

$$w_{ck} = C_{wk}\left(\cosh\left(\frac{\lambda_m x}{L}\right)-\cos\left(\frac{\lambda_m x}{L}\right)-\gamma_m\left(\sinh\left(\frac{\lambda_m x}{L}\right)-\sin\left(\frac{\lambda_m x}{L}\right)\right)\right)e^{i\omega t}, \quad k=(0,1,2) \tag{49}$$

$$\cos\lambda_m.\cosh\lambda_m = -1; \quad \lambda_m = 1.875, 4.694, 7.854, 10.995, 14.137 \tag{50}$$

$$\gamma_m = \frac{\sinh\lambda_m - \sin\lambda_m}{\cosh\lambda_m - \cos\lambda_m} \quad m=(1,2,3,...) \tag{51}$$

where "$a_m = m\pi/L$"; "m" depicts the wave number and "$C_{uk}, C_{wk}, C_{\phi j}$" are the unknown constants. The nine equations are displayed as matrix form as follows:

$$(k_m - N_0 \times G_m)C_m = 0 \tag{52}$$

Nine eigen vectors are Cm; "G" is the geometric matrix and "K" is the stiffness matrix. In order to validate the results of the present approach, they are compared with the results of literatures (Vo et al., 2014) and (Vo et al., (2015)), which are shown in Table 1 and Table 2, for the simply supported (S-S) and clamped (C-F) boundary conditions. It' seen that there are good agreements between the present results and the literatures.

Table 1
Critical load parameters of present results and literatures (Vo et al., 2014) and (Vo et al., (2015)) for (S-S)

N	Theory	2-1-2	1-1-1	1-8-1
	L/h=5			
0	Vo et al. (HOBT) (Vo et al., 2014)	48.5959	48.5959	48.5959
	Vo et al. (quasi-3D) (Vo et al., (2015))	49.5906	49.5906	49.5906
	Present	50.7611	50.7611	50.7611
1	Vo et al. (HOBT) (Vo et al., 2014)	22.2108	24.5596	38.7838
	Vo et al. (quasi-3D) (Vo et al., (2015))	22.7065	25.1075	39.6144
	Present	23.0681	25.1621	39.8011
	L/h=20			
0	Vo et al. (HOBT) (Vo et al., 2014)	53.2364	53.2364	53.2364
	Vo et al. (quasi-3D) (Vo et al., (2015))	53.3145	53.3145	53.3145
	Present	55.7922	55.7922	55.7922
1	Vo et al. (HOBT) (Vo et al., 2014)	23.4211	25.9588	41.9004
	Vo et al. (quasi-3D)	23.4572	25.9989	41.9639
	Present	23.5221	26.0847	41.0498

Table 2
Critical load parameters of present results and literatures (Vo et al., 2014) and (Vo et al., (2015)) for (C-F)

N	Theory	2-1-2	1-1-1	1-8-1

		L/h=5		
0	Vo et al. (HOBT) (Vo et al., 2014)	13.0594	13.0594	13.0594
	Vo et al. (quasi-3D) (Vo et al., (2015))	13.1224	13.1224	13.1224
	Present	13.3934	13.3934	13.3934
1	Vo et al. (HOBT) (Vo et al., 2014)	5.7921	6.4166	10.3093
	Vo et al. (quasi-3D) (Vo et al., (2015))	5.8244	6.4516	10.3581
	Present	5.9931	6.6112	10.3973
		L/h=20		
0	Vo et al. (HOBT) (Vo et al., 2014)	13.3730	13.3730	13.3730
	Vo et al. (quasi-3D) (Vo et al., (2015))	13.3981	13.3981	13.3981
	Present	13.4421	13.4421	13.4421
1	Vo et al. (HOBT) (Vo et al., 2014)	5.8713	6.5083	10.5174
	Vo et al. (quasi-3D) (Vo et al., (2015))	5.8832	6.5214	10.5375
	Present	6.0257	6.7978	10.7712

To investigate the numerical results, two models of sandwich beams are considered. The functionally graded layers are made of Silicon nitride and Stainless steel as ceramic and metal phases which gradually distributed across the thickness. To see the thermal constants of the material properties in Eq. (1) refer to reference (Reddy, (2003)). Sandwich structures are introduced based on the thickness of the layers. For example, 1-4-1 sandwich is a structure that the core thickness is four times of the skins thicknesses. To simplify the results, the non-dimensional critical load parameter is presented as:

$$N_{cr} = \frac{N_0}{10^9} \tag{53}$$

The material properties of structures are affected in high temperature conditions. The critical load parameter changing via the temperature for different models of 1-8-1 sandwich beams with clamped-free boundary condition is shown in Fig. 2. Geometrical parameters are “h=0.02m, L/h=5, m=1”. Based on Eq. (1), when temperature is raised, Elastic modulus of constituent reduces. As a result, the panels strength decreases, which is an important factor of reducing the critical load in thermal surrounding. In the case of N=0, the functionally graded layers are composed of ceramic only, so, the thermal resistant and stability against the high temperature conditions are more than the other values of “N”, so its critical load parameters are higher than others. When “N” is increased, the percentage of ceramic decreases in the layers which affects the material properties. So, stability, stiffness and buckling load of the sandwich beams reduces. In 1-8-1 model, since ceramic of sandwich type-II which has a FG core is higher than the type-I, the stiffness, resistant and the critical buckling load of the type-II is higher and this type of sandwich is more sensitive in changing the “N”. In both sandwiches and in the higher value of “N”, the percentage of ceramic tend to zero, so the stability of the beams decreases impressively. In sandwich type-I, when “N=0”, by rising the temperature, the critical load parameter reduces 74.93%, for “N=1” and “N=2” it decreases 85.55%, and 89.52%, respectively. And in sandwich type-II, when “N=0”, by increasing the temperature, the critical load parameter decreases 53.84%, for “N=1” and “N=2” it decreases 69.54%, and 73.15%, respectively.

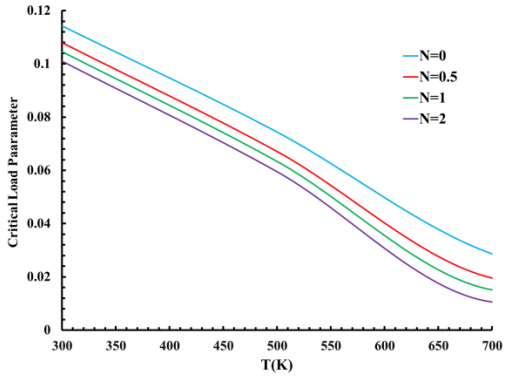

a. sandwich Type-I

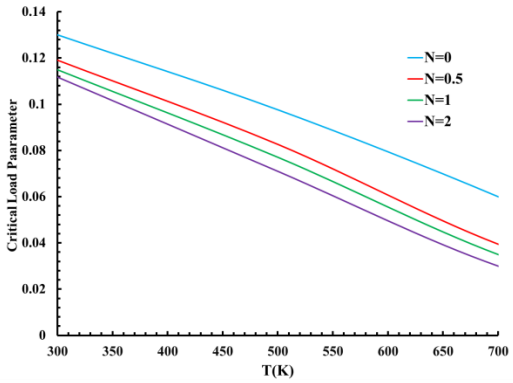

b. sandwich Type-II

Fig .2. Critical load changing with temperature in FG sandwich beams.

Length and thickness are important parameters in the sandwich beams. Effect of a non-dimensional ratio of length (L/h) to thickness on the buckling load is depicted in Fig. 3. Geometrical parameters are “h = 0.02m, T=300K, m=1” in the 1-8-1 FG sandwich beams. Increasing the ratio in a constant “N” leads to decrease the stability of the structure and the critical load parameter. So, it shouldn’t be considered the long length in

structures. It has been shown that in sandwich type-I, the critical load parameters are lower than sandwich type-II. Also, it is obvious that, by rising the "N", the critical load parameters decrease, but in this case effect of variation of the length is dominant parameter and its variation has an impressive effect on the stability. For example, in sandwich type-I, for "L/h=5", by increasing "N", the critical load parameter decrease 11.60%, but for "N=0", by increasing this ratio, the critical load parameter decreases 4267%. And, in sandwich type-II, for "L/h=5", by increasing "N", the critical load parameter decrease 14.06%, but for "N=0", by increasing this ratio, the critical load decreases 4367%. Also, it should be noted that when the ratio is more than 12, the slope of the variation of the critical load decrease significantly.

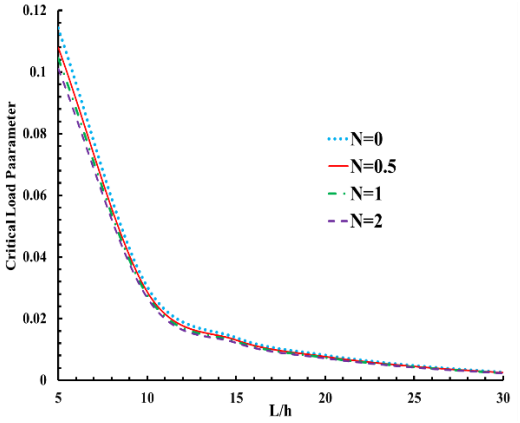

a. sandwich Type-I

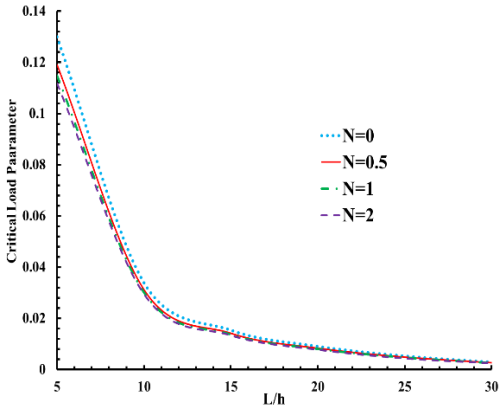

b. sandwich Type-II

Fig .3. Critical load changing with L/h ratio in the FG sandwich beams.

Effect of the core to skins thickness ratio, "h_c/h_t", on the critical load in a constant total thickness is shown in Fig. 4 for different "N". Geometrical parameters are "h=0.02m, T=300K, m=1, L/h=10". "h_c/h_t=0.5" shows that the thickness of the core is half of the skins thicknesses, which refers to 2-1-2 sandwich. Also, "h_c/h_t=8" refers to 1-8-1 sandwich. The highest percentage of ceramic is in the 2-1-2 sandwich type-I. By rising the ratio, ceramic decreases and the panels become softer, so the critical load parameter reduces. Also it is obvious that, the 2-1-2 case has more ceramic than 1-8-1 one, so buckling load of 2-1-2 is higher. There are different results in sandwich type-II. 1-8-1 case has the most ceramic. In a constant thickness, when the ratio is raised, the percentage of ceramic increases at the lower "N", especially in "N=0". Also, it is obvious that the critical buckling load in 1-8-1 is higher than 2-1-2, due to the ceramic amount. As shown in the Fig. 4, after a certain value of "N", when "N" is increased, 2-1-2 case has a higher critical load than 1-8-1 one. It means that in a constant thickness, after that value of "N", increasing the "N" results in the lower ceramic in FG layers, so at all ratio, the critical load parameters reduce in both model of sandwich beams. For sandwich type-I, in "h_c/h_t=0.5", the critical load parameter decreases 14.82% when "N" is increased, and in "h_c/h_t=8", the critical load parameter decrease 12.17% when "N" is increased. Also, for "N=0", by increasing this ratio, the critical load decreases 19.87%, but for "N=2", it decreases 17.38%. For sandwich type-II, in "h_c/h_t=0.5", the critical load parameter decrease 0.692% when "N" is increased, and in "h_c/h_t=8", the critical load parameter decrease 13.42% when "N" is increased. Also, for "N=0", by increasing this ratio, the critical load increases 8.79%, but for "N=2", it decreases 5.14%.

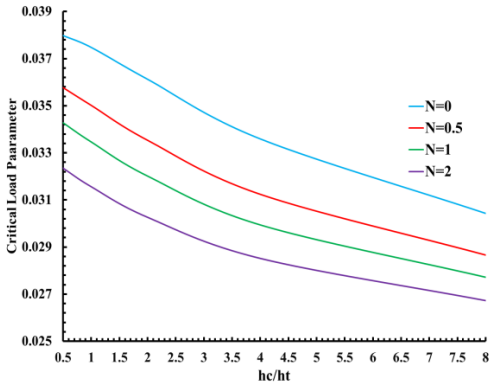

a. sandwich Type-I

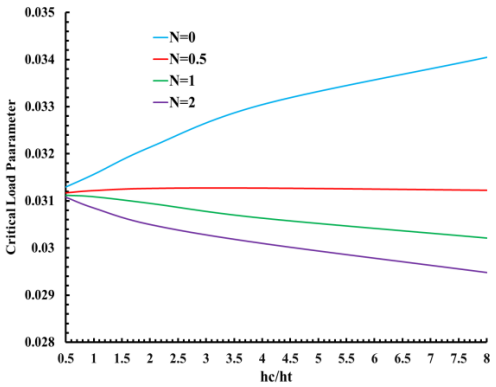

b. sandwich Type-II

Fig .4. Critical load changing via the "hc/ht" ratio in FG sandwich beams.

The total thickness of beam changing effect, “h”, on the critical load parameter for different “N”, and is shown in Fig. 5. Geometrical parameters are “T=300K, m=1, L/h=10”. It is obvious that by rising the “h” in the constant “L/h”, the critical load parameter decreases. The slope of reducing the critical load in lower than 0.02m is high for both models of sandwich, but in the larger “h”, the slope of reducing is lower. It means after a certain value, rising the thickness has a little effect on the critical load. For example, when “L/h=10” and “N=0”, by increasing the “h”, the critical load decrease 2292.43% for sandwich type-I, and 2345.86% for sandwich type-II. But, it is seen that after the “h=0.02m”, the rate of variation is decreased for both sandwiches. For “h=0.01m”, by increasing “N”, the critical load parameter decrease 11.60% for sandwich type-I and 14.06% for sandwich type-II.

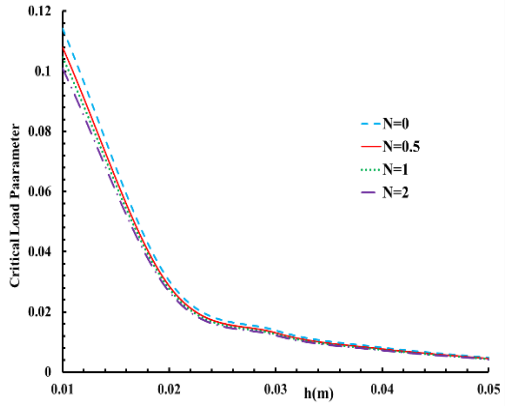

a. sandwich Type-I

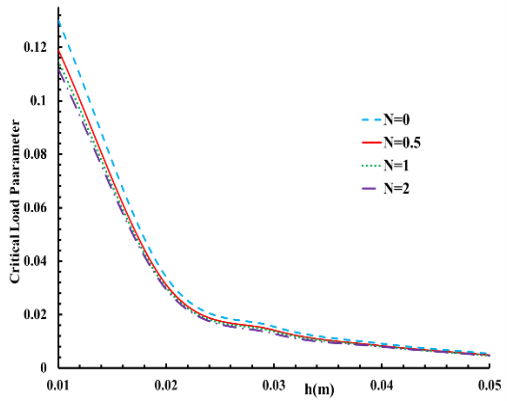

b. sandwich Type-II

Fig .5. Critical load changing via thickness in FG sandwich beams.

The wave number, “m”, effect on the critical load parameters for in different “N” and constant total thickness is shown in the Fig. 6. Geometrical parameters are “h=0.02m, T=300K, m=1, L/h=10”. It is obvious that increasing the wave number increases the critical load parameters. Although in the lower wave numbers, the critical load parameter of both sandwiches are close to each other, but in the larger “m”, the critical load parameters in the sandwich type-II are higher.

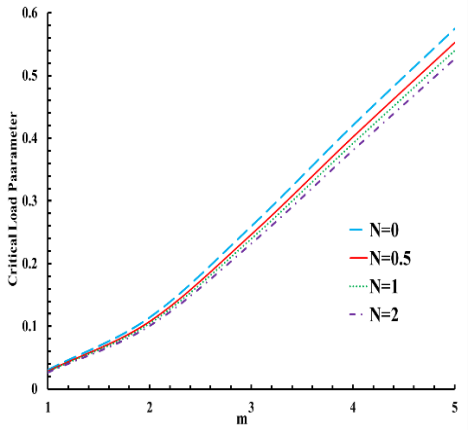

a. sandwich Type-I

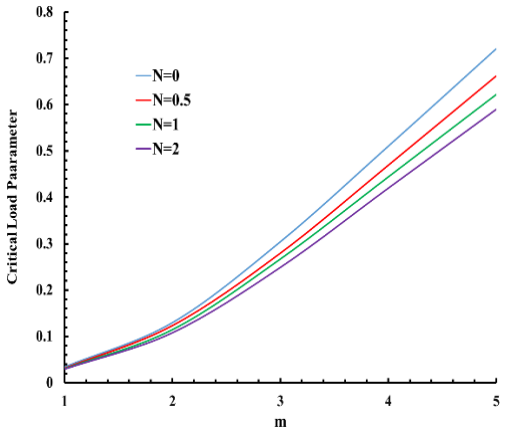

b. sandwich Type-II

Fig .6. Critical load changing via wave number.

To show the porosity effect on the critical load, two porosity distributions, even and uneven, are investigated, which shown in Fig 7. And Fig. 8. It is clear that, in both models of beam, by rising the porosity volume fraction, the critical load parameter decreases. In the even porosity distribution, the decreasing of the critical load is more than uneven one for both models of sandwich beam. It is considered that the voids are spread across the cross section in the even case, but these voids are piled up in the central area of the cross section in the uneven case. In sandwich type-I, and for the even case and “N=0”, by increasing the volume fraction of the porosity, the critical load decreases 26.47%, and in the uneven case in “N=0”, by increasing the volume fraction of the porosity, the critical load decreases 13.54%. And, in sandwich type-II, and for the even case and “N=0”, by increasing the volume fraction of the porosity, the critical load decreases 22.61%, and in the uneven case in “N=0”, by increasing the volume fraction of the porosity, the critical load decreases 5.89%.

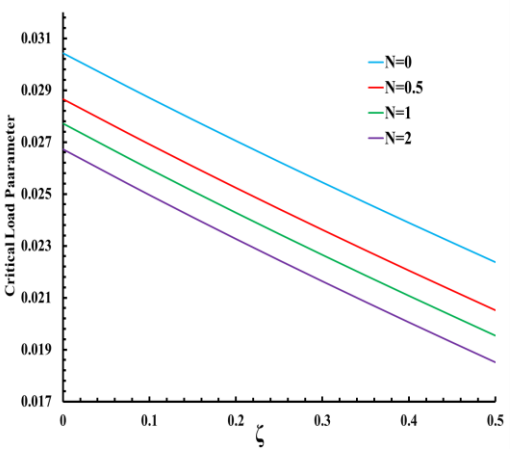

a. sandwich Type-I

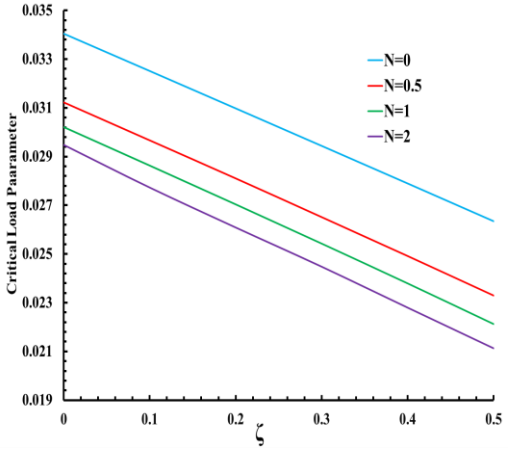

b. sandwich Type-II

Fig .7. Critical load changing via even porosity.

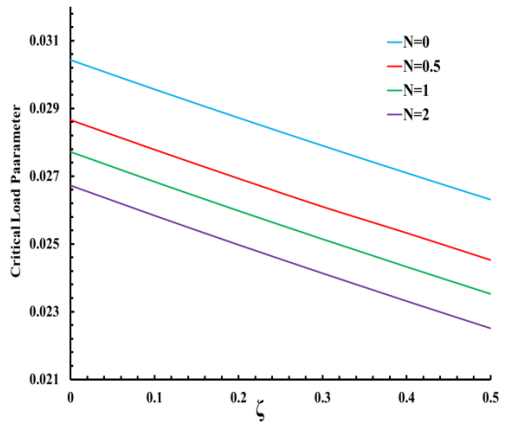

a. sandwich Type-I

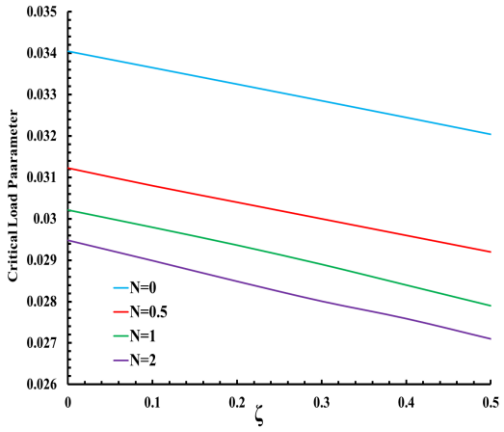

b. sandwich Type-II

Fig .8. Critical load changing via uneven porosity.

4. Conclusion

Analyzing the buckling behavior of the sandwich beams with functionally graded material faces and homogeneous core and with functionally graded material core and homogeneous faces were discussed in this paper based on a high order sandwich beam theory. Properties of constituent materials were considered temperature dependent and functionally graded materials were modelled by adding porosity effects. Minimum potential energy principle and Galerkin method were used to obtain and solve the equations in a clamped-free boundary conditions. Lateral displacement, and thermal stresses of the core and Lagrange strains were considered. Thickness, length, porosity, wave number and temperature effect on the critical load were investigated too. By studying the results it is concluded that:

- When the temperature is raised, the critical load parameters reduce.
- In thermal surrounding, FG core sandwich beams have higher stability and resistant than FG faces ones.
- When the power law index is raised, the critical load parameters reduce.
- When the length to thickness ratio is increased, the critical load parameter reduce.
- In FG face sandwich beams, when the core to skin thickness ratio is raised, the critical load parameters reduce. In FG core sandwich beams, at the lower “N”, the critical load parameters increase, but after a special value of “N”, when power law index is increased, the critical load parameters reduce.
- When the total thickness is increased, the critical load parameters reduce.
- When the wave number is raised, the critical load parameter increases.

- When the amount of the both porosities are increased, the critical load parameters reduce. Critical load changing in even model is larger than uneven one.

References

[1] Akbaş, Ş.D., (2015). On post-buckling behavior of edge cracked functionally graded beams under axial loads. *International Journal of Structural Stability and Dynamics* 15, 1450065.

[2] Alijani, A., Darvizeh, M., Darvizeh, A., Ansari, R., (2015). Elasto-plastic pre-and post-buckling analysis of functionally graded beams under mechanical loading. *Proceedings of the Institution of Mechanical Engineers, Part L: Journal of Materials: Design and Applications* 229, 146-165.

[3] Almitani, K.H., (2018). Buckling behaviors of symmetric and antisymmetric functionally graded beams. J*ournal of Applied and Computational Mechanics* 4, 115-124.

[4] Basaglia, C., Camotim, D., (2015). Buckling analysis of thin-walled steel structural systems using generalized beam theory (GBT). *International Journal of Structural Stability and Dynamics* 15, 1540004.

[5] Bhangale, R.K., Ganesan, N., (2006). Thermoelastic buckling and vibration behavior of a functionally graded sandwich beam with constrained viscoelastic core. *Journal of Sound and Vibration* 295, 294-316.

[6] Chai, G., Yap, C., Lim, T., (2010). Bending and buckling of a generally laminated composite beam-column. *Proceedings of the Institution of Mechanical Engineers, Part L: Journal of Materials: Design and Applications* 224, 1-7.

[7] Challamel, N., Girhammar, U.A., (2011). Variationally-based theories for buckling of partial composite beam–columns including shear and axial effects. *Engineering structures* 33, 2297-2319.

[8] CW, Y., Chai, G., Parlapalli, M.S.R., (2008). Effect of flexural stiffness estimates on the buckling load of delaminated composite beams. *Proceedings of the Institution of Mechanical Engineers, Part L: Journal of Materials: Design and Applications* 222, 91-102.

[9] Dinzart, F., Molinari, A., Herbach, R., (2008). Thermomechanical response of a viscoelastic beam under cyclic bending; self-heating and thermal failure. *Archives of Mechanics* 60, 59-85.

[10] Fouda, N., El-Midany, T., Sadoun, A., (2017). Bending, buckling and vibration of a functionally graded porous beam using finite elements. *Journal of applied and computational mechanics* 3, 274-282.

[11] Frostig, Y., Baruch, M., Vilnay, O., Sheinman, I., (1992). High-order theory for sandwich-beam behavior with transversely flexible core. *Journal of Engineering Mechanics* 118, 1026-1043.

[12] Gao, C.-F., Pan, Y.-H., Zhang, W., Rao, J.-X., Huang, Y., (2021). Buckling of two-directional functionally graded cylindrical beams based on a high-order cylindrical beam model. *International Journal of Structural Stability and Dynamics*, 2150099.

[13] Hamed, M.A., Mohamed, S.A., Eltaher, M.A., (2020). Buckling analysis of sandwich beam rested on elastic foundation and subjected to varying axial in-plane loads. *Steel and Composite Structures* 34, 75-89.

[14] Janevski, G., Despenić, N., Pavlović, I., (2020). Thermal buckling and free vibration of Euler-Bernoulli FG nanobeams based on the higher-order nonlocal strain gradient theory. *Archives of Mechanics* 72.

[15] Kheirikhah, M., Khalili, S., Fard, K.M., (2012). Biaxial buckling analysis of soft-core composite sandwich plates using improved high-order theory. *European Journal of Mechanics-A/Solids* 31, 54-66.

[16] Koissin, V., Shipsha, A., Skvortsov, V., (2010). Effect of physical nonlinearity on local buckling in sandwich beams. *Journal of Sandwich Structures & Materials* 12, 477-494.

[17] Li, C., Shen, H.-S., Wang, H., (2019). Thermal post-buckling of sandwich beams with functionally graded negative Poisson's ratio honeycomb core. *International Journal of Mechanical Sciences* 152, 289-297.

[18] Liu, Y., Su, S., Huang, H., Liang, Y., (2019). Thermal-mechanical coupling buckling analysis of porous functionally graded sandwich beams based on physical neutral plane. *Composites Part B: Engineering* 168, 236-242.

[19] Magnucki, K., Smyczyński, M., Jasion, P., (2013). Deflection and strength of a sandwich beam with thin binding layers between faces and a core. *Archives of Mechanics* 65, 301-311.

[20] Majumdar, A., Das, D., (2018). A study on thermal buckling load of clamped functionally graded beams under linear and nonlinear thermal gradient across thickness. *Proceedings of the Institution of Mechanical Engineers, Part L: Journal of Materials: Design and Applications* 232, 769-784.

[21] Malikan, M., (2019). On the buckling response of axially pressurized nanotubes based on a novel nonlocal beam theory. *Journal of Applied and Computational Mechanics* 5, 103-112.

[22] Mayandi, K., Jeyaraj, P., (2015). Bending, buckling and free vibration characteristics of FG-CNT-reinforced polymer composite beam under non-uniform thermal load. *Proceedings of the Institution of Mechanical Engineers, Part L:*

Journal of Materials: Design and Applications 229, 13-28.

[23] Osofero, A.I., Vo, T.P., Nguyen, T.-K., Lee, J., (2016). Analytical solution for vibration and buckling of functionally graded sandwich beams using various quasi-3D theories. *Journal of Sandwich Structures & Materials* 18, 3-29.

[24] Paul, A., Das, D., (2017). A study on non-linear post-buckling behavior of tapered Timoshenko beam made of functionally graded material under in-plane thermal loadings. *The Journal of Strain Analysis for Engineering Design* 52, 45-56.

[25] Rahmani, M., Dehghanpour, S., (2020). Temperature-Dependent Vibration of Various Types of Sandwich Beams with Porous FGM Layers. *International Journal of Structural Stability and Dynamics*, 2150016.

[26] Rahmani, M., Mohammadi, Y., (2021). Vibration of two types of porous FG sandwich conical shell with different boundary conditions. *Structural Engineering and Mechanics* 79, 401-413.

[27] Rahmani, M., Mohammadi, Y., Kakavand, F., (2019)-a. Vibration analysis of sandwich truncated conical shells with porous FG face sheets in various thermal surroundings. *Steel and Composite Structures* 32, 239-252.

[28] Rahmani, M., Mohammadi, Y., Kakavand, F., (2020)-a. Buckling analysis of different types of porous FG conical sandwich shells in various thermal surroundings. *Journal of the Brazilian Society of Mechanical Sciences and Engineering* 42, 1-16.

[29] Rahmani, M., Mohammadi, Y., Kakavand, F., Raeisifard, H., (2019)-b. Buckling behavior analysis of truncated conical sandwich panel with porous FG core in different thermal conditions. *Amirkabir Journal of Mechanical Engineering* 52, 141-150.

[30] Rahmani, M., Mohammadi, Y., Kakavand, F., Raeisifard, H., (2020)-b. Vibration analysis of different types of porous FG conical sandwich shells in various thermal surroundings. *Journal of Applied and Computational Mechanics* 6, 416-432.

[31] Reddy, J.N., (2003). *Mechanics of laminated composite plates and shells: theory and analysis*. CRC press.

[32] Scirè Mammano, G., Dragoni, E., (2017). Mechanical design of buckled beams for low-stiffness elastic suspensions: Theory and application. *Proceedings of the Institution of Mechanical Engineers, Part L: Journal of Materials: Design and Applications* 231, 140-150.

[33] Tran, T.T., Nguyen, N.H., Do, T.V., Minh, P.V., Duc, N.D., (2019). Bending and thermal buckling of unsymmetric functionally graded sandwich beams in high-temperature environment based on a new third-order shear deformation theory. *Journal of Sandwich Structures & Materials*, 1099636219849268.

[34] Vo, T.P., Thai, H.-T., Nguyen, T.-K., Inam, F., Lee, J., (2015). A quasi-3D theory for vibration and buckling of functionally graded sandwich beams. *Composite Structures* 119, 1-12.

[35] Vo, T.P., Thai, H.-T., Nguyen, T.-K., Maheri, A., Lee, J., (2014). Finite element model for vibration and buckling of functionally graded sandwich beams based on a refined shear deformation theory. *Engineering structures* 64, 12-22.